Cake Properties of Nanocolloid Evaluated by Variable Pressure Filtration Associated with Reduction in Cake Surface Area

Eiji Iritani, Nobuyuki Katagiri, and Ryota Nakajima
Dept. of Chemical Engineering, Nagoya University, Furo-cho, Chikusa-ku, Nagoya 464-8603, Japan

Kuo-Jen Hwang and Tung-Wen Cheng
Dept. of Chemical and Materials Engineering, Tamkang University, Tamsui, New Taipei City 25137, Taiwan

DOI 10.1002/aic.14601
Published online September 16, 2014 in Wiley Online Library (wileyonlinelibrary.com)

A potential method has been developed for evaluating simultaneously both the average specific resistance and average porosity of the filter cake formed in unstirred dead-end ultrafiltration of nanocolloids such as bovine serum albumin solution and silica sol. The method consists of variable pressure filtration followed by constant pressure filtration. The relation between the average specific cake resistance and the pressure drop across the cake was determined from the evolution of the filtration rate with time in the course of the variable pressure filtration period, based on the compressible cake filtration model. The average porosity was evaluated from the significant flux decline caused by a sudden reduction in the cake surface area in the middle of the constant pressure filtration period. The pressure dependences of both the average specific cake resistance and average cake porosity were obtained from only two runs which differed from each other in the pressure profiles. © 2014 American Institute of Chemical Engineers *AIChE J*, 60: 3869–3877, 2014
Keywords: ultrafiltration, variable pressure filtration, cake surface area, specific cake resistance, porosity

Introduction

Ultrafiltration of nanocolloids, for example, protein solutions and suspensions of nanoparticles, has attracted a considerable amount of attention in such widely diversified fields as not only chemical processing, and the dairy and food industry but also nanotechnology, biotechnology, biomedicine, drinking water production, treatment of domestic and industrial effluents, production of water suitable for reuse, and so on. A dramatic flux reduction observed in ultrafiltration processes known as membrane fouling is identified as the dominant feature contributing to deterioration of ultrafiltration performance. One of the critical factors governing such membrane fouling may be the buildup of highly resistant filter cake caused by the accumulation of macrosolutes and nanoparticles rejected by the membrane during ultrafiltration,[1–7] in addition to pore constriction and/or pore blockage within the membrane.[8] Therefore, an understanding of the nature of the filter cake formed on the membrane surface can serve as a basis for clarifying the real mechanism of ultrafiltration and mitigating the membrane fouling. Among cake properties, both the average specific cake resistance α_{av}, which is closely connected to the filterability, and average cake porosity ε_{av}, which is related to the cake dryness, are recognized as by far the most important key factors controlling ultrafiltration behaviors,[3,9–12] as is the case with traditional cake filtration of particulate suspensions.[13–16] In particular, knowledge about dependences of α_{av} and ε_{av} on the pressure drop Δp_c across the highly compressible filter cake, which are obtained from dead-end ultrafiltration tests, is essential for the design of new and operating existing ultrafilter equipment.

The relation between α_{av} and Δp_c can be generally obtained from a series of constant pressure filtration tests conducted under several filtration pressures, or a constant rate filtration test,[17] on the basis of the existing compressible cake filtration model.[18–21] The step-up pressure filtration test in which the applied pressure is increased incrementally during filtration can be used as an alternative test procedure for determining α_{av} as a function of the pressure.[22] Variable pressure filtration tests in which neither pressure nor filtration rate (flux) are maintained constant can also offer information about the pressure dependence of α_{av} from the monitoring of the filtration rate vs. pressure characteristics.[23] Recently, the single constant pressure filtration test was developed to employ a filter medium with an extremely high hydraulic resistance compared to the resistance of the filter cake formed, resulting in the observable time variation of Δp_c, and thus the pressure dependence of α_{av} was evaluated over a wide range of Δp_c from only one test.[23–25] On the basis of this principle, the single step-up pressure filtration test in which the pressure was increased in stages in the course of filtration was developed to obtain the pressure dependence of α_{av} of the filter cake formed in ultrafiltration of nanocolloids over a much wider range of Δp_c from only one test.[26]

Correspondence concerning this article should be addressed to E. Iritani at iritani@nuce.nagoya-u.ac.jp.

Also, a technique has been developed for accurately determining ε_{av} in constant pressure filtration on the principle of a sudden reduction in the filtration area of the cake surface during the course of filtration.[27] In the test, ε_{av} was evaluated based on an abrupt decrease in the filtration rate caused by a sudden reduction in the cake surface area during the course of filtration associated with a decrease in the inner cross-sectional area of the test cell. The method was regarded as a potential tool for accurately evaluating cake porosity not only in filtration of particulate suspension[27,28] but also in ultrafiltration of protein solution.[3,29] Also in vacuum filtration, a filter equipped with a floating disk was used to produce the phenomenon of a sudden reduction in the cake surface area during filtration.[30] A method has been developed for determining the relation between ε_{av} and Δp_c by measuring the variation with time of hydraulic pressure distributions across the filter cake in step-up pressure filtration.[22] However, the measurement of the hydraulic pressure is quite laborious and requires much skill. The dependence of ε_{av} on Δp_c was evaluated from a step-up pressure filtration test on the basis of the multistage reduction of the cake surface area during filtration using a filter in which the inner cross-sectional area decreases with the distance from the filter medium in stages.[31] However, the reliability of this method for highly compressible cakes is severely decreased by the consolidation of the preformed filter cake caused by a sudden reduction in the cake surface area.

Moreover, to our knowledge a filtration testing method remains to be developed for simultaneously evaluating the dependences of α_{av} and ε_{av} on Δp_c from minimal experimental runs despite the large number of investigations of nanocolloid ultrafiltration. Therefore, the immediate development of the method for efficiently analyzing the cake characteristics largely depending on the pressure drop across the cake has been eagerly anticipated. Knowledge of the cake properties such as α_{av} and ε_{av} serves as a basis for elucidating the fouling mechanism in ultrafiltration of nanocolloids and has important implications for the design and operation of industrial ultrafiltration systems worked under a variety of pressure conditions, also contributing to the determination of optimum pressure conditions.

In the present article, a potential method is explored for simply and accurately evaluating both the average specific resistance α_{av} and average porosity ε_{av} of filter cake formed in dead-end ultrafiltration of nanocolloids as functions of the pressure drop Δp_c across the filter cake from only two runs. The method is based on variable pressure filtration followed by constant pressure filtration associated with a sudden reduction in the cake surface area during the course of filtration. The effect of pressure on α_{av} can be determined from the flux decline behavior controlled by time-dependent pressure during the variable pressure filtration period, and ε_{av} corresponding to a constant pressure can be evaluated from the flux decline behavior in the constant pressure filtration period. The method can accurately evaluate the pressure dependence of both the average specific cake resistance and average cake porosity over wide pressure ranges from only two sets of filtration tests. This advantage of the method is substantiated from a comparison with a series of conventional constant pressure filtration tests in which the filtration area are suddenly reduced during filtration.[27]

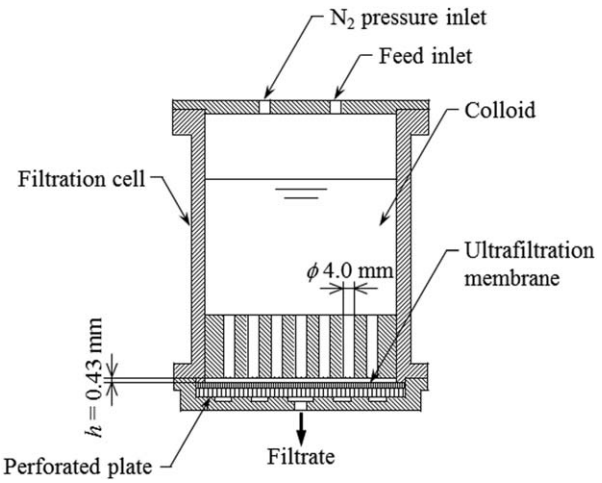

Figure 1. Schematic view of filtration cell used in this research.

Experimental

Materials

The solutes used in the experiments were bovine serum albumin (BSA) (Fraction V, Sigma-Aldrich, Japan) with a molecular weight of about 67 kDa and an isoelectric point of about pH 5.1 and silica sol (Snowtex(ST)-XS, Nissan Chemical Industries) with a nominal mean diameter of 6.4 nm. The values of the density ρ_s of solutes were 1364 and 2150 kg/m^3 for BSA molecules and silica particles, respectively.[32] The particle-size distribution of silica sol was measured by a dynamic light scattering (DLS) photometer (DLS-8000, Otsuka Electronics), resulting in the mean specific surface area size of 4.8 nm.

Dilute aqueous colloids were prepared by dispersing preweighed quantities of the solutes or solutions in ultrapure, deionized water (resistivity of at least 18 MΩ cm) prepared by purifying tap water through ultrapure water systems equipped both with Elix-UV20 and with Milli-Q Advantage for laboratory use (Millipore). In the BSA solution make-up, the pH was adjusted to 5.1 of the isoelectric point by adding small amounts of 0.1 M NaOH or HCl. The BSA concentration by weight was adjusted to 5.0×10^{-3} and the concentration of silica sol was kept at 0.01 and 0.03.

Experimental apparatus and technique

An unstirred batch filtration cell with an effective membrane area of 24.63 cm^2 was used in this research and the experiments were carried out in the dead-end mode. To evaluate the average porosity ε_{av} of the filter cake, the filtration area was suddenly reduced from 24.63 to 4.65 cm^2 by constructing the orifice structure at the distance h of 0.43 mm from the membrane surface, as shown in Figure 1. In the experiments, the applied filtration pressure was adjusted automatically by a computer-driven electronic pressure regulator by applying compressed nitrogen gas and was increased in accordance with

$$p = p_1 + (p_{max} - p_1)\left(\frac{\theta}{\theta_c}\right)^q; \quad \theta \le \theta_c \tag{1}$$

where p is the applied filtration pressure, p_1 is the initial filtration pressure, p_{max} is the final filtration pressure, θ is the filtration time, θ_c is the filtration time when operation moves from variable pressure to constant pressure filtration, and q

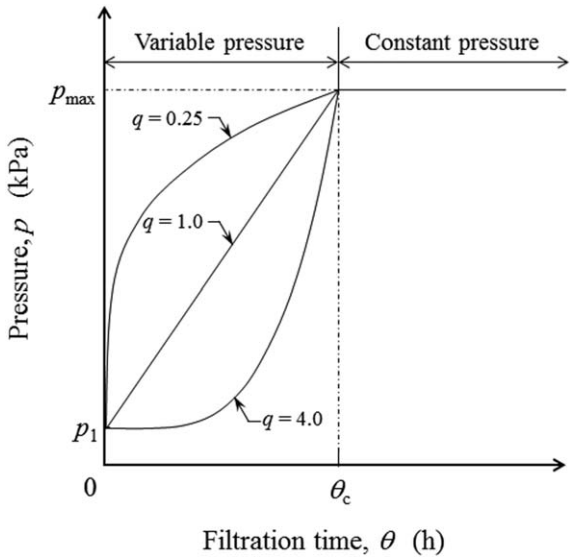

Figure 2. Rising patterns in pressure in variable pressure filtration period.

is the parameter controlling the rate of increase in the filtration pressure. To examine the influence of rising behaviors of applied filtration pressure in the variable filtration period on the pressure dependence of α_{av} obtained, 4.0, 1.0, and 0.25 were selected as the values of q and the corresponding time-dependent pressure profiles are illustrated in Figure 2. Depending on the filterability of nanocolloids, the values of θ_c were set to 5 and 3 h for BSA solution and silica sol, respectively. Once the filtration pressure p was at its peak, p_{max}, at the time θ_c, constant pressure filtration was continued at the pressure of p_{max}. Asymmetric regenerated cellulose ultrafiltration membranes (Millipore) with a nominal molecular weight cutoff of 10 kDa were used to ensure the complete rejection of both solutes.

The filtrate was collected in a reservoir placed on an electronic balance (Shimadzu) connected to a personal computer to collect and record mass vs. time data during the filtration test. The weights were converted to volumes using density correlations in order to determine the relation between the cumulative filtrate volume v per unit effective membrane area and the filtration time θ and thus the relation between the filtration rate ($dv/d\theta$) and v (or ($dv/d\theta$) and θ).

For comparison, a series of constant pressure filtration tests were performed under different filtration pressure conditions ranging from 49 to as high as 490 kPa, using the same filter as that used in variable pressure filtration tests developed in this research.

Results and Discussion

Flux decline behaviors

Typical data of variable pressure filtration examined in this study are plotted in Figure 3 in the form of the reciprocal filtration rate ($d\theta/dv$) against the cumulative filtrate volume v per unit effective membrane area. It should be noted that the term ($d\theta/dv$) is a measure of the total filtration resistance R_t, as described by Darcy's law in the form[33]

$$\frac{1}{u_1} = \frac{d\theta}{dv} = \frac{\mu R_t}{p} \tag{2}$$

where u_1 is the filtration rate and μ is the viscosity of the filtrate.

Starting with an initial pressure p_1 of 10 kPa, the applied filtration pressure is increased to the final pressure p_{max} of 98 kPa during the variable pressure filtration period of the first stage. The rise in the pressure is controlled according to Eq. 1 in which $\theta_c = 5$ h and $q = 4.0$. The pressure is then maintained at p_{max} and thus constant pressure filtration follows variable pressure filtration. The value of the cumulative filtrate volume per unit effective membrane area, v_c, at the transition point from variable pressure to constant pressure filtration is 0.82 cm, as shown in the figure. The variation of $d\theta/dv$ with v depends critically on the increase both in the cake resistance and the filtration pressure as the driving force in filtration during the variable pressure filtration period. The increase in the cake resistance with the progress of filtration accelerates the flux decline, whereas the increase in the pressure enlarges the flux. Initially, $d\theta/dv$ increases with v, largely influenced by the increase in the cake resistance because the pressure increase is not so marked in the first portion of filtration. However, as variable pressure filtration proceeds, $d\theta/dv$ signifies a slight decline owing to a rapid increase in the pressure.

In this study, the compressible cake filtration model is of use in the description of the dead-end ultrafiltration behaviors and in the evaluation of the properties of the filter cake exhibiting compressible behavior. Basically, the compressible cake filtration model can adequately describe the increase in the hydraulic resistance to flow caused by the cake buildup during the course of dead-end ultrafiltration, implicitly assuming that all the colloidal particles convected toward the membrane accumulate on the surface in dead-end ultrafiltration.[11] Therefore, the temporal behavior of the hydraulic resistance attributed to the developing filter cake can be evaluated from the relation between the filtration rate and the applied filtration pressure. According to the compressible cake filtration model, the evolution of the filtration rate with v is described by[23,34]

$$\frac{1}{u_1} = \frac{d\theta}{dv} = \frac{\mu\alpha_{av}\rho s}{p(1-ms)}v + \frac{\mu R_m}{p} \tag{3}$$

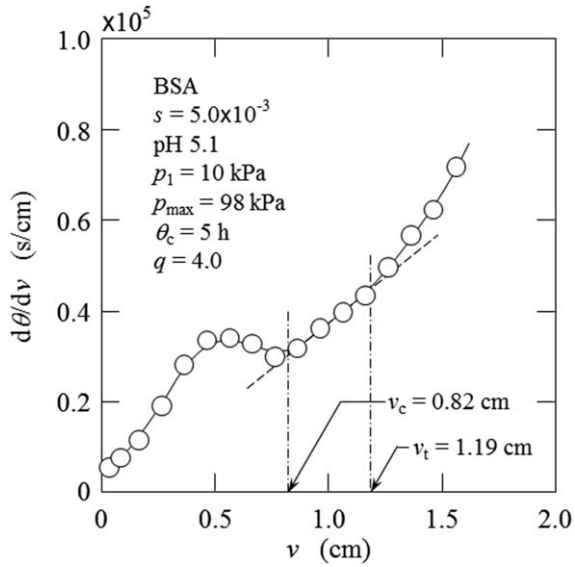

Figure 3. Relation between reciprocal filtration rate and filtrate volume per unit effective membrane area in ultrafiltration of BSA solution.

where α_{av} is the average specific cake resistance, which is the quantitative measurement of the filterability of the colloids, ρ is the density of the filtrate, s is the mass fraction of solutes in the solution, and m is the ratio of the mass of wet to mass of dry cake. The latter is related to the average porosity ε_{av} in the filter cake by[14]

$$m=1+\frac{\rho\varepsilon_{av}}{\rho_s(1-\varepsilon_{av})} \tag{4}$$

In Eq. 3, R_m is the hydraulic resistance provided by the membrane and is given by[26]

$$R_m=\frac{p_1}{\mu}\left(\frac{d\theta}{dv}\right)_m \tag{5}$$

where $(d\theta/dv)_m$ is the reciprocal filtration rate at the beginning of filtration when no cake is present.

The effective pressure drop Δp_c across the filter cake is written as

$$\Delta p_c=p-\Delta p_m=p-\mu R_m u_1 \tag{6}$$

where Δp_m is the liquid pressure drop across the membrane. Eliminating R_m in Eq. 6 by means of Eq. 5 leads to

$$\Delta p_c=p-\frac{(d\theta/dv)_m}{(d\theta/dv)}p_1 \tag{7}$$

Consequently, if the pressure dependence of m in Eq. 3 (or ε_{av} in Eq. 4) is known, then the use of Eqs. 3 and 7 permits the calculation of the relation between α_{av} and Δp_c on the basis of the value of instantaneous reciprocal filtration rate $(d\theta/dv)$ for a given v-value during variable pressure filtration. If the term $(1-ms)$ is approximated by unity in filtration conducted with dilute solutions, Eq. 3 reduces to

$$\frac{1}{u_1}=\frac{d\theta}{dv}=\frac{\mu\alpha_{av}\rho s}{p}v+\frac{\mu R_m}{p} \tag{8}$$

In that case, it is possible to evaluate the relationship of α_{av} on Δp_c readily from Eqs. 7 and 8 without information about the cake dryness.

As shown in Figure 3, $d\theta/dv$ varies linearly with v once filtration progresses under the constant pressure condition of p_{max}. In the case of constant pressure filtration, Eq. 3 takes the familiar form

$$\frac{1}{u_1}=\frac{d\theta}{dv}=\frac{2}{K_v}v+\frac{\mu R_m}{p} \tag{9}$$

where K_v is the Ruth coefficient of constant pressure filtration defined as[35]

$$K_v=\frac{2p(1-ms)}{\mu\rho s\alpha_{av}} \tag{10}$$

The term K_v is viewed as constant in constant pressure filtration with negligible resistance of the membrane compared to the cake resistance, suggesting that the pressure drop Δp_c across the cake is approximated by the applied pressure p. It is possible to obtain the dependence of α_{av} on Δp_c from the data points of $d\theta/dv$ vs. v also in the constant pressure filtration period of the second stage in the same way as variable pressure filtration period of the first stage. However, it can be also determined directly from the slope of the linear relationship between $d\theta/dv$ vs. v using Eqs. 9 and 10.

Subsequently, the moment the surface of the filter cake reaches to the position where the inner cross-sectional area

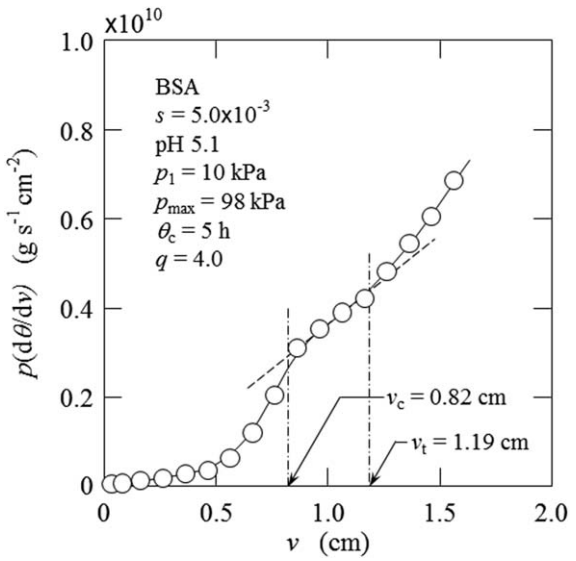

Figure 4. Relation between reciprocal filtration rate multiplied by applied filtration pressure and filtrate volume per unit effective membrane area in ultrafiltration of BSA solution.

of the filtration cell cylinder is reduced abruptly, the filtrate flow rate drops off dramatically due to the substantial decrease in the surface area of the growing filter cake. As a consequence, the plot of $d\theta/dv$ against v deviates markedly from the previous linear relationship under the constant pressure condition after v is beyond the critical value v_t of 1.19 cm in this case, and $d\theta/dv$ undergoes a more rapid increase, as shown in Figure 3. With the use of the value of v_t thus obtained, the average porosity ε_{av} of the filter cake corresponding to a constant pressure of 98 kPa can be calculated by writing the following overall mass balance of dead-end filtration in which the total mass of colloid is equal to the sum of the mass of cake and the mass of filtrate

$$\frac{\rho_s h(1-\varepsilon_{av})}{s}=\{\rho_s h(1-\varepsilon_{av})+\rho h\varepsilon_{av}\}+\rho v_t \tag{11}$$

Equation 11 is rewritten as

$$\varepsilon_{av}=\frac{\rho_s h(1-s)-\rho s v_t}{\rho_s h(1-s)+\rho s h} \tag{12}$$

where h is the distance from the membrane surface to the position where the filtration area is reduced, and is equal to the cake thickness when v reaches v_t.

The applied filtration pressure p varies with the progress of filtration during variable pressure filtration period. To distinguish the variation of the specific cake resistance α_{av} with p during variable pressure filtration period in the plot of flux decline data, Eq. 3 is advantageously rewritten as

$$p\left(\frac{1}{u_1}\right)=p\left(\frac{d\theta}{dv}\right)=\frac{\mu\alpha_{av}\rho s}{(1-ms)}v+\mu R_m \tag{13}$$

Figure 4 represents $d\theta/dv$ multiplied by p against v based on the experimental data presented in Figure 3. The value of $p(d\theta/dv)$ increases monotonically with increasing v during the variable pressure filtration period in sharp contrast to the plot shown in Figure 3, suggesting that the average specific cake resistance gradually increases corresponding to the

increase in the filtration pressure with the progress of variable pressure filtration.

Pressure dependences of α_{av} and ε_{av} in filter cake

It is well known that the average specific resistance α_{av} and average porosity ε_{av} of the filter cake are substantially dependent on the pressure drop Δp_c across the cake according to the compressible cake filtration model.[18–21,25] Recently, the model has been utilized in order to elucidate the mechanism of dead-end ultrafiltration.[3,4,9] Several empirical expressions have been available to represent α_{av} as a function of Δp_c for compressible filter cake. Typical available expressions are as follows[26]

$$\alpha_{av} = \alpha_1 \Delta p_c^{\,n_1} \tag{14}$$

$$\alpha_{av} = \frac{a_0(1-n_2)(\Delta p_c/p_{a1})}{(1+\Delta p_c/p_{a1})^{1-n_2}-1} \tag{15}$$

$$\alpha_{av} = a_1\left(1+\frac{\Delta p_c}{p_{a2}}\right)^{n_3} \tag{16}$$

where α_1, a_0, a_1, p_{a1}, p_{a2}, n_1, n_2, and n_3 are the empirical constants. Equation 14 describes the linearity in the logarithmic plot of α_{av} vs. Δp_c, and the local specific cake resistance α is assumed constant below some low pressure p_i.[14,36] Equations 15 and 16 can fit the experimental data more accurately over a wide range up to extremely low pressures and can describe similar curves of α_{av} vs. Δp_c.[3,18] Also, for the solidosity (volume fraction of solids) $(1-\varepsilon_{av})$ of the filter cake, the similar functions can be empirically applied as follows[37]

$$1-\varepsilon_{av} = (1-\varepsilon_1)\Delta p_c^{\,\beta_1} \tag{17}$$

$$1-\varepsilon_{av} = \frac{(1-\varepsilon_2)(1-n_2-\beta_2)\left\{(1+\Delta p_c/p_{a1})^{1-n_2}-1\right\}}{(1-n_2)\left\{(1+\Delta p_c/p_{a1})^{1-n_2-\beta_2}-1\right\}} \tag{18}$$

$$1-\varepsilon_{av} = (1-\varepsilon_3)\left(1+\frac{\Delta p_c}{p_{a2}}\right)^{\beta_3} \tag{19}$$

where ε_1, ε_2, ε_3, β_1, β_2, and β_3 are the empirical constants. It should be noted that p_{a1} in Eq. 15 and p_{a2} in Eq. 16 are identical to p_{a1} in Eq. 18 and p_{a2} in Eq. 19, respectively.[37] In this research, Eqs. 16 and 19, which can fit closely with the experimental data by simpler expressions, are used to represent α_{av} and $(1-\varepsilon_{av})$ as functions of Δp_c.

Figure 5 illustrates the flow diagram of the model algorithm used in calculating the parameters in Eqs. 16 and 19 from the experimental data. Initially, the relation between α_{av} and Δp_c is obtained from the data of $d\theta/dv$ vs. v using Eqs. 7 and 8, and the adjustable parameters of a_1, p_{a2}, and n_3 in Eq. 16 are determined by fitting to the α_{av} vs. Δp_c data. Subsequently, two pairs of data points of $(1-\varepsilon_{av})$ vs. Δp_c are obtained from two experiments conducted under different values of the applied pressure in the later constant pressure period, and one can calculate the values of ε_3 and β_3 in Eq. 19 because the value of p_{a2} in Eq. 19 is previously obtained in determining the relational expression of α_{av} vs. Δp_c given by Eq. 16. Next, the relation between α_{av} and Δp_c is modified according to Eqs. 3, 4, and 7 taking the cake porosity into account, and the relational expression between ε_{av} and Δp_c is also recalculated on the basis of the value of p_{a2} newly obtained. Such an iterative calculation is repeated until the value of α_{av} corresponding to each Δp_c coincides within the range of predetermined accuracy before and after the calculation of one loop.

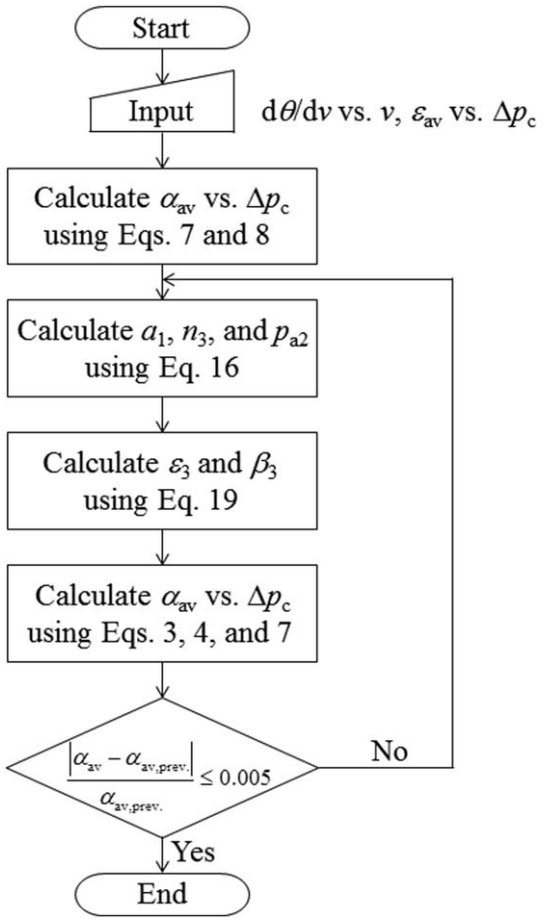

Figure 5. Flow diagram of model algorithm used in calculating parameters in Eqs. 16 and 19 from experimental data.

It should be noted that at least two experimental runs are necessary to determine the pressure dependence of ε_{av} because ε_{av} corresponding to the final filtration pressure p_{max} can be determined from an experimental run. Figures 6 and 7 illustrate the dependences of α_{av} and $(1-\varepsilon_{av})$ on Δp_c obtained from two experiments conducted under the condition that $p_1 = 10$ kPa and $p_{max} = 98$ kPa and the condition that $p_1 = 49$ kPa and $p_{max} = 490$ kPa. Plots shown in Figure 6 are obtained using the aforementioned method in consideration of the cake porosity ε_{av} (i.e., the ratio of the mass of wet to mass of dry cake, m) shown in Eq. 3. The plots are essentially identical (within 2.4–7.4%) to those obtained directly from Eq. 8 in place of Eq. 3 without the necessity of using the values of the cake porosity ε_{av}, although the latter are not shown in the figure in order to avoid the overlap of plots. The specific cake resistance α_{av} is determined over a wide range of pressures from a low of 2 to a high of 490 kPa. Data indicate that the increase in Δp_c results in an increase in α_{av} and a decrease in ε_{av}. It is found that the logarithmic plot of α_{av} vs. Δp_c shows a linear relationship at pressures over more than approximately 40 kPa. Below that pressure the plots are concave upward. The solid curves in Figures 6 and 7 are the calculations obtained using Eqs. 16 and 19, respectively, and are fairly consistent with the experimental data over the entire pressure range. For comparison,

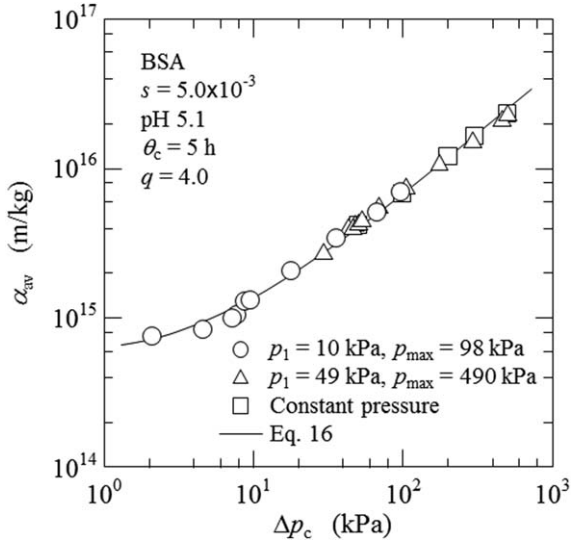

Figure 6. Pressure dependence of average specific cake resistance in ultrafiltration of BSA solution.

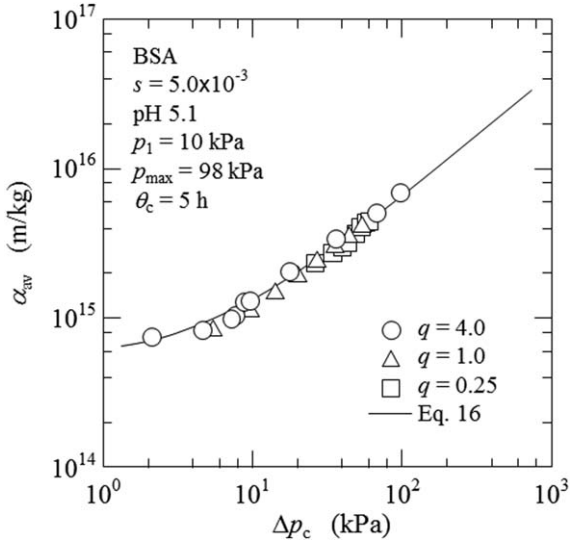

Figure 8. Influence of rising rate in pressure in variable pressure filtration period on pressure dependence of average specific cake resistance in ultrafiltration of BSA solution.

the plots are included in the graphs for the data obtained from a series of constant pressure filtration experiments conducted at different pressures (from 49 to 490 kPa) and are in excellent agreement with those obtained from the method presented in this study for the straight-line portion of the logarithmic plots in the relatively high pressure region. It is interesting to note that the pressure dependence of both α_{av} and ε_{av} in the filter cake are accurately determined from only two experimental runs according to the method developed here.

The influence of rising behaviors of applied filtration pressure in the variable pressure filtration period on the experimental result, particularly the pressure dependence of α_{av}, is examined for three patterns illustrated in Figure 2 and the results are illustrated in Figure 8 in the form of α_{av} against Δp_c. In either experiment, the filtration pressure is increased from the initial pressure p_1 of 10 kPa to the final pressure p_{max} of 98 kPa for 5 h. But, the rising rate in the pressure differs from pattern to pattern by assigning 0.25, 1.0, or 4.0 to q in Eq. 1. With $q = 4.0$, the dependence of α_{av} on Δp_c is obtained up to the lower pressure range because the rising rate in the pressure is more gradual in that pressure range. It would be, therefore, recommended to increase the filtration pressure as slow as possible in the very early stage of variable pressure filtration in order to determine the values of α_{av} in a wide range of pressures. Accordingly, the experiments are carried out under the condition that $q = 4.0$, except for the results shown in this figure.

Contrary to the two experiments shown in Figures 6 and 7, another two experiments are conducted under the condition that $p_1 = 10$ kPa and $p_{max} = 20$ kPa and the condition that $p_1 = 49$ kPa and $p_{max} = 294$ kPa, in order to establish the criterion of selecting the pressure conditions in this method. The results are provided in Figures 9 and 10.

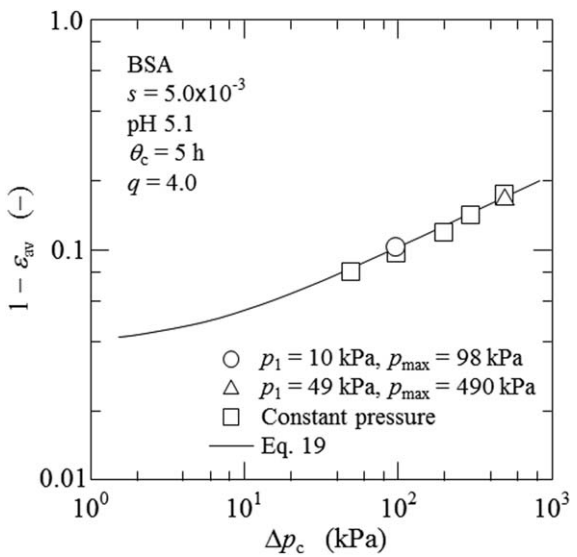

Figure 7. Pressure dependence of average cake solidosity in ultrafiltration of BSA solution.

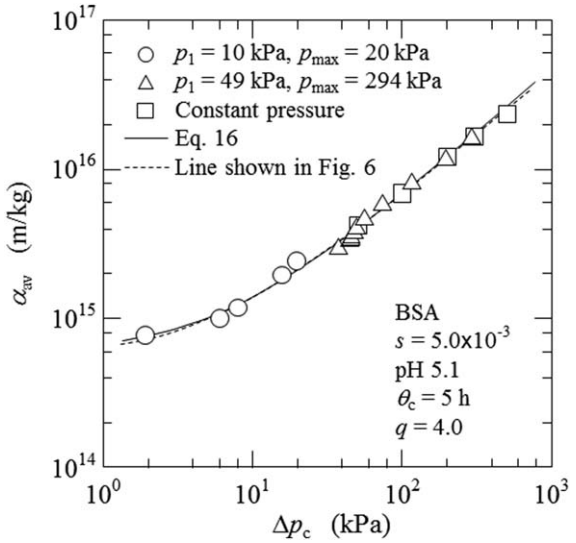

Figure 9. Pressure dependence of average specific cake resistance obtained from variable pressure filtration data that are different from those shown in Figure 6.

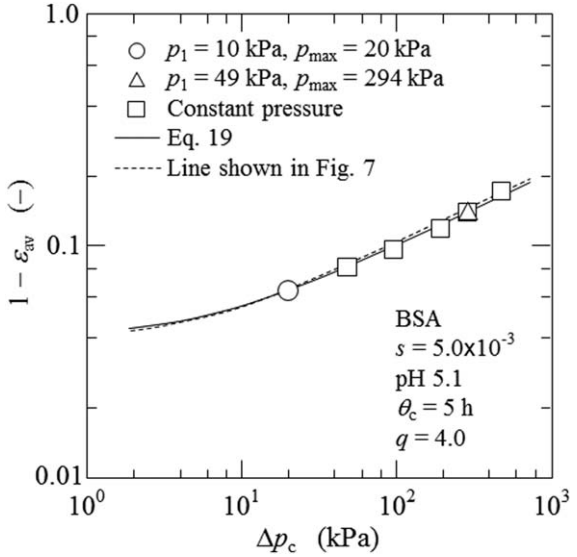

Figure 10. Pressure dependence of average cake solidosity obtained from variable pressure filtration data that are different from those shown in Figure 7.

Figure 9 illustrates the relation between α_{av} and Δp_c. The solid lines in the figure are the calculations fitted to the experimental data using Eq. 16. In contrast, the dotted line in Figure 9 is the calculations shown in Figure 6. Both calculations are reasonably in step with each other. Also concerning the relation between $(1 - \varepsilon_{av})$ and Δp_c, similar results are obtained, as depicted in Figure 10. This indicates the high accuracy of the method for determining the dependence of α_{av} and $(1 - \varepsilon_{av})$ on Δp_c presented in this study. In addition, an important point to note is that the values of the two final pressures used in the two experiments should be dramatically different in order to obtain the experimental data of $(1 - \varepsilon_{av})$ vs. Δp_s over a wide range of pressures.

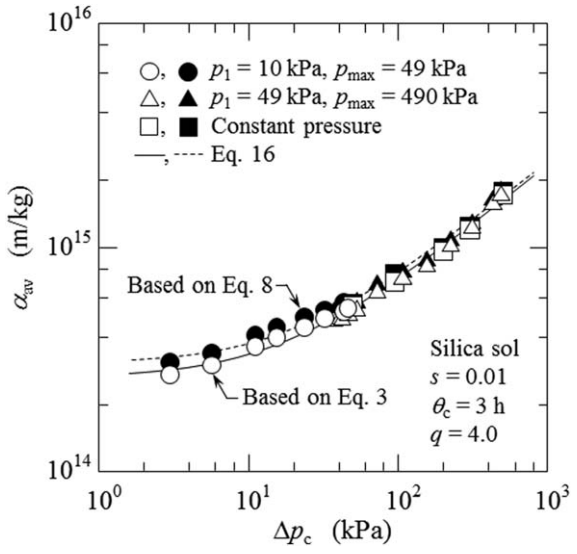

Figure 11. Pressure dependence of average specific cake resistance in ultrafiltration of silica sol at mass fraction of 0.01.

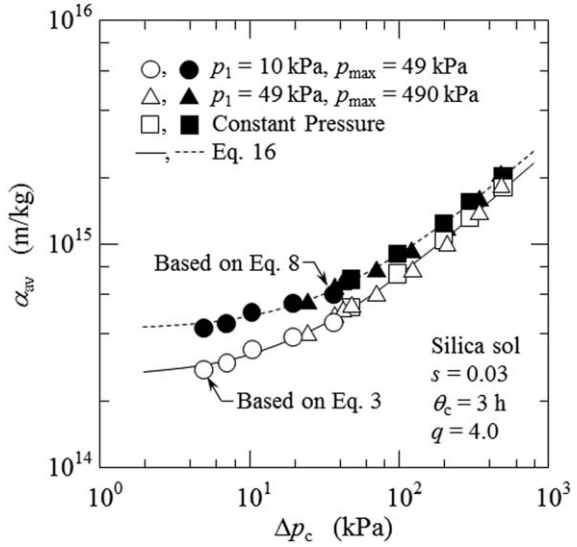

Figure 12. Pressure dependence of average specific cake resistance in ultrafiltration of silica sol at mass fraction of 0.03.

Effect of feed concentration on cake properties

To ascertain the effect of feed concentration on filtration behaviors, nanocolloid of silica sol is selected as a test sample solution as silica sol can be prepared at a much higher concentration than BSA solution. Figures 11 and 12 show the dependences of α_{av} on Δp_c at the mass fractions s of 0.01 and 0.03, respectively. The filled circles in both figures are the calculations obtained using Eq. 8 in place of Eq. 3 on the assumption that the term $(1 - ms)$ is approximated by unity, while the open circles are the calculations obtained using Eq. 3 in consideration of the accurate values of $(1 - ms)$. The solid and dotted curves are the calculations fitted to the open and filled circles using Eq. 16, respectively.

The solid curve lies below the dotted curve for each concentration as the values of α_{av} decrease by considering the accurate values of $(1 - ms)$, and this tendency is marked particularly at low pressures. If $(1 - ms)$ term is neglected, there

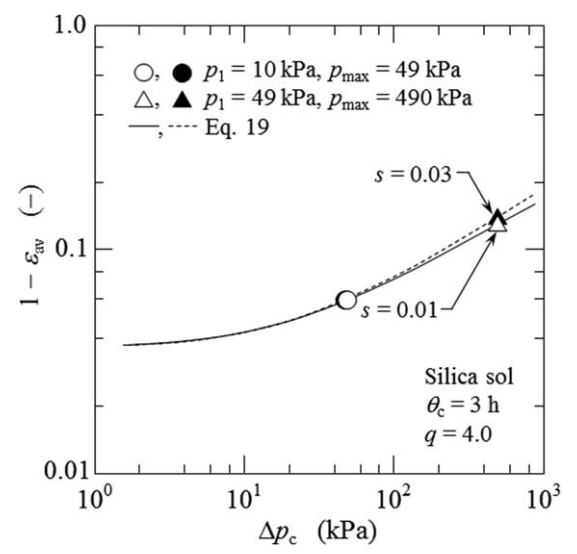

Figure 13. Pressure dependence of average cake solidosity in ultrafiltration of silica sol at mass fractions of 0.01 and 0.03.

are clear differences between the values of α_{av} obtained by Eqs. 3 and 8 when the feed concentration is high. However, if $(1 - ms)$ term is included in the calculation, the measured α_{av} values are not impacted by the feed concentration, as is obvious from the comparison of the open circles shown in Figures 11 and 12. This indicates that it is necessary to measure the pressure dependence of $(1 - \varepsilon_{av})$ in order to accurately determine the dependence of α_{av} on the pressure.

Figure 13 compares the dependences of $(1 - \varepsilon_{av})$ on Δp_c for silica sol at mass concentrations of 0.01 and 0.03. The open and filled data points in the figure represent the results for mass concentrations of 0.01 and 0.03, respectively. It is also found that the plots give close agreement with each other independent of the values of the solution concentration tested, as in the case of the relation between α_{av} and Δp_c. The solid and dotted lines are fits to the open and filled data points obtained using Eq. 19, respectively.

Conclusions

Variable pressure filtration followed by constant pressure filtration, in sequence, was accomplished in the dead-end mode by filtering nanocolloids with an ultrafiltration membrane using a filter in which the filtration area was suddenly reduced, in order to determine the cake properties of nanocolloids in membrane filtration. The flux decline behaviors during the variable pressure filtration period of the preceding stage in filtration were utilized to obtain the relation between the average specific cake resistance and the pressure drop across the cake on the basis of the compressible cake filtration model. Subsequently, the average cake porosity corresponding to the applied filtration pressure during the constant pressure filtration period of the later stage was evaluated from an abrupt flux decline brought about by the effect of a sudden reduction in the surface area of the filter cake during the course of filtration. Only two sets of filtration tests enabled us to accurately evaluate the pressure dependence of both the average specific cake resistance and average cake porosity over wide pressure ranges. More accurate values of the average specific cake resistance were determined with the aid of the pressure dependence of the average cake porosity. The results derived from the method developed in this research were compared with constant pressure filtration data collected for a variety of filtration pressures using a filter equipped with the structure of the sudden reduction in the filtration area, excellent agreement being observed.

Acknowledgments

This work has been partially supported by a Grant-in-Aid for Scientific Research from The Ministry of Education, Culture, Sports, Science and Technology, Japan and from The Ministry of the Environment, Japan, and by The Steel Foundation for Environmental Protection Technology. The authors wish to acknowledge with sincere gratitude the financial support leading to the publication of this article.

Notation

a_0 = empirical constant in Eq. 15, m/kg
a_1 = empirical constant in Eq. 16, m/kg
$(d\theta/dv)_m$ = reciprocal filtration rate at beginning of filtration, s/m
h = distance from membrane surface to position where filtration area is reduced, m
K_v = Ruth coefficient of constant pressure filtration, m^2/s
m = ratio of mass of wet to mass of dry cake
n_1 = empirical constant in Eq. 14
n_2 = empirical constant in Eq. 15
n_3 = empirical constant in Eq. 16
p = applied filtration pressure, Pa
p_{a1} = empirical constant in Eq. 15, Pa
p_{a2} = empirical constant in Eq. 16, Pa
p_i = some low pressure below which local specific cake resistance α is kept constant, Pa
p_{max} = final filtration pressure, Pa
p_1 = initial filtration pressure, Pa
q = exponent in Eq. 1
R_m = hydraulic resistance of membrane, m^{-1}
R_t = total filtration resistance, m^{-1}
s = mass fraction of solutes in colloid
u_1 = filtration rate, m/s
v = cumulative filtrate volume per unit effective membrane area, m^3/m^2
v_c = cumulative filtrate volume per unit effective membrane area at transition point from variable pressure to constant pressure filtration, m^3/m^2
v_t = cumulative filtrate volume per unit effective membrane area collected until filter cake surface reaches reduced surface, m^3/m^2

Greek letters

α = local specific cake resistance, m/kg
α_{av} = average specific cake resistance, m/kg
α_1 = empirical constant in Eq. 14, $kg^{-n_1-1}m^{1+n_1}s^{2n_1}$
β_1 = empirical constant in Eq. 17
β_2 = empirical constant in Eq. 18
β_3 = empirical constant in Eq. 19
Δp_c = pressure drop across filter cake, Pa
Δp_m = liquid pressure drop across membrane, Pa
ε_{av} = average porosity of filter cake
ε_1 = empirical constant in Eq. 17
ε_2 = empirical constant in Eq. 18
ε_3 = empirical constant in Eq. 19
θ = filtration time, s
θ_c = filtration time when operation moves from variable pressure to constant pressure filtration, s
μ = viscosity of filtrate, Pa s
ρ = density of filtrate, kg/m^3
ρ_s = density of solutes, kg/m^3

Literature Cited

1. Reihanian H, Robertson CR, Michaels AS. Mechanism of polarization and fouling of ultrafiltration membranes by proteins. *J Membr Sci*. 1983;16:237–258.
2. Suki A, Fane AG, Fell CJD. Flux decline in protein ultrafiltration. *J Membr Sci*. 1984;21:269–283.
3. Iritani E, Nakatsuka S, Aoki H, Murase T. Effect of solution environment on unstirred dead-end ultrafiltration characteristics of proteinaceous solutions. *J Chem Eng Jpn*. 1991;24:177–183.
4. Nakakura H, Yamashita A, Sambuichi M, Osasa K. Electrical conductivity measurement of filter cake in dead-end ultrafiltration of protein solution. *J Chem Eng Jpn*. 1997;30:1020–1025.
5. Mohammadi T, Kohpeyma A, Sadrzadeh M. Mathematical modeling of flux decline in ultrafiltration. *Desalination*. 2005;184:367–375.
6. Sarkar B. A combined complete pore blocking and cake filtration model during ultrafiltration of polysaccharide in a batch cell. *J Food Eng*. 2013;116:333–343.
7. Thekkedath A, Naceur WM, Kecili K, Sbai M, Elane A, Auret L, Suty H, Machinal C, Pontié M. Macroscopic and microscopic characterization of a cellulosic ultrafiltration (UF) membrane fouled by a humic acid cake deposit: first step for intensification of reverse osmosis (RO) pre-treatments. *C R Chim*. 2007;10:803–812.
8. Iritani E. A review on modeling of pore-blocking behaviors of membranes during pressurized membrane filtration. *Dry Technol*. 2013;31:146–162.
9. Iritani E, Hattori K, Murase T. Analysis of dead-end filtration based on ultracentrifugation method. *J Membr Sci*. 1993;81:1–13.
10. Iritani E, Hattori K, Murase T. Evaluation of dead-end ultrafiltration properties by ultracentrifugation method. *J Chem Eng Jpn*. 1994;27:357–362.

11. Iritani E, Mukai Y, Hagihara E. Measurements and evaluation of concentration distributions in filter cake formed in dead-end ultrafiltration of protein solutions. *Chem Eng Sci*. 2002;57:53–62.
12. Lodge B, Judd SJ, Smith AJ. Characterisation of dead-end ultrafiltration of biotreated domestic wastewater. *J Membr Sci*. 2004;231:91–98.
13. Tiller FM, Cooper HR. The role of porosity in filtration: IV. *Constant pressure filtration. AIChE J*. 1960;6:595–601.
14. Tiller FM, Cooper H. The role of porosity in filtration: Part V. *Porosity variation in filter cakes. AIChE J*. 1962;8:445–449.
15. Mendret J, Guigui C, Schmitz P, Cabassud C. In situ dynamic characterization of fouling under different pressure conditions during dead-end filtration: compressibility properties of particle cakes. *J Membr Sci*. 2009;333:20–29.
16. Loginov M, Citeau M, Lebovka N, Vorobiev E. Evaluation of low-pressure compressibility and permeability of bentonite sediment from centrifugal consolidation data. *Sep Purif Technol*. 2012;92:168–173.
17. Shirato M, Aragaki T, Mori R, Sawamoto K. Predictions of constant pressure and constant rate filtrations based upon an approximate correction for side wall friction in compression permeability cell data. *J Chem Eng Jpn*. 1968;1:86–90.
18. Shirato M, Murase T, Iritani E, Tiller FM, Alciatore AF. Filtration in the chemical process industry. In: Matteson MJ, Orr C, editors. *Filtration: Principles and Practices*. New York: Marcel Dekker, Inc., 1987:299–420.
19. Olivier J, Vaxelaire J, Vorobiev E. Modelling of cake filtration: an overview. *Sep Sci Technol*. 2007;42:1667–1700.
20. Tarleton ES, Wakeman RJ. *Solid/Liquid Separation: Equipment Selection and Process Design*. Oxford: Elsevier, Ltd., 2007.
21. Shirato M, Sambuichi M, Kato H, Aragaki T. Internal flow mechanism in filter cakes. *AIChE J*. 1969;15:405–409.
22. Murase T, Iritani E, Cho JH, Shirato M. Determination of filtration characteristics based upon filtration tests under step-up pressure conditions. *J Chem Eng Jpn*. 1989;22:373–378.
23. Iritani E, Katagiri N, Kanetake S. Determination of cake filtration characteristics of dilute suspension of bentonite from various filtration tests. *Sep Purif Technol*. 2012;92:143–151.
24. Iritani E, Katagiri N, Takaishi Y, Kanetake S. Determination of pressure dependence of permeability characteristics from single constant pressure filtration test. *J Chem Eng Jpn*. 2011;44:14–23.
25. Chen W. Analysis of compressible suspensions for an effective filtration and deliquoring. *Dry Technol*. 2006;24:1251–1256.
26. Iritani E, Katagiri N, Tsukamoto M, Hwang KJ. Determination of cake properties in ultrafiltration of nano-colloids based on single step-up pressure filtration test. *AIChE J*. 2014;60:289–299.
27. Murase T, Iritani E, Cho JH, Nakanomori S, Shirato M. Determination of filtration characteristics due to sudden reduction in filtration area of filter cake surface. *J Chem Eng Jpn*. 1987;20:246–251.
28. Murase T, Iritani E, Cho JH, Shirato M. Determination of filtration characteristics of power-law non-Newtonian fluids-solids mixtures under constant-pressure conditions. *J Chem Eng Jpn*. 1989;22:65–71.
29. Iritani E, Mukai Y, Murase T. Properties of filter cake in dead-end ultrafiltration of binary protein mixtures with retentive membranes. *Trans IChemE A: Chem Eng Res Des*. 1995;73:551–558.
30. Iritani E, Mukai Y, Cho JH. Evaluation of compression-permeability characteristics based on vacuum filtration test using nutsche equipped with floating disc. *J Soc Powder Technol Jpn*. 2001;38:548–554.
31. Iritani E, Nagaoka H, Katagiri N. Determination of filtration characteristics of yeast suspension based upon multistage reduction in cake surface area under step-up pressure conditions. *Sep Purif Technol*. 2008;63:379–385.
32. Iritani E, Katagiri N, Murakami Y, Nakano D. Measurements of growth rate of filter cake in vertical single-pass ultrafiltration using hollow fiber membrane module. *Sep Purif Technol*. 2012;47:2281–2289.
33. Iritani E, Katagiri N, Sengoku T, Yoo KM, Kawasaki K, Matsuda A. Flux decline behaviors in dead-end microfiltration of activated sludge and its supernatant. *J Membr Sci*. 2007;300:36–44.
34. Tiller FM, Crump JR, Ville F. A revised approach to the theory of cake filtration. *Proceedings of the International Symposium on Fine Particles Processing, Vol. 2*. 1980:1549–1582.
35. Ruth BF. Studies in filtration. III. Derivation of general filtration equations. *Ind Eng Chem*. 1935;27:708–723.
36. Sperry DR. Note and correspondence: a study of the fundamental laws of filtration using plant-scale equipment. *Ind Eng Chem*. 1921;13:1163–1164.
37. Tiller FM, Lue WF. Basic data fitting in filtration. *J Chin Inst Chem Eng*. 1980;11:61–70.

Manuscript received Mar. 27, 2014, and revision received July 24, 2014.